Biosensors and Bioelectronics 128 (2019) 151–158

Contents lists available at ScienceDirect

Biosensors and Bioelectronics

journal homepage: www.elsevier.com/locate/bios

A highly integrated real-time digital PCR device for accurate DNA quantitative analysis

Shufang Zhou[a,1], Tong Gou[a,1], Jiumei Hu[a,b], Wenshuai Wu[a,b], Xiong Ding[a,b], Weibo Fang[a], Zhenming Hu[a], Ying Mu[a,b,*]

[a] Research Center for Analytical Instrumentation, Institute of Cyber-Systems and Control, State Key Laboratory of Industrial Control Technology, Zhejiang University, Hangzhou 310027, PR China
[b] College of Life Sciences, Zhejiang University, Hangzhou 310058, Zhejiang, PR China

ARTICLE INFO

Keywords:
Real-time digital PCR
Raspberry Pi
Microfluidic chip
Absolute quantitative accuracy

ABSTRACT

Misclassification of positive partitions in microfluidic digital polymerase chain reaction (dPCR) can cause the false positives and false negatives, which significantly alter the resulting estimate of target DNA molecules. To address this issue, establishing real-time fluorescence interrogation of each partition in microfluidic arrays is an effective way in which false positive and false negative partitions can be eliminated. However, currently available devices for real-time fluorescence interrogation are either not competent for microfluidic digital array, or they are bulky, expensive and entail peripheral equipment due to low integration. Therefore, in this study, a Raspberry Pi based, low-cost and highly integrated device is presented to achieve real-time fluorescence detection for microfluidic digital array, termed real-time dPCR device. In the device, uniform thermocycler, streamlined real-time fluorescence imaging setup, and compact data processing system are all integrated to undergo on-chip dPCR amplification, real-time fluorescence detection, and data analysis. Using this real-time dPCR device, the accuracy of DNA absolute quantification by dPCR is improved, since the misclassification of positive partitions is efficiently reduced based on the characteristic real-time fluorescence curves of positive partitions in a self-priming microfluidic chip. Compared with end-point dPCR on our device and commercialized QuantStudio™ 3D dPCR system, the real-time dPCR on our device exhibits a higher accuracy for DNA quantification. In addition, this real-time dPCR device is much smaller and cheaper than the commercialized Digital PCR system, but not sacrificing the capability of error correction for absolute quantitation analysis. Conclusively, this highly integrated real-time dPCR device is very beneficial for DNA quantitative analysis where the determination accuracy is pivotal.

1. Introduction

Digital polymerase chain reaction (dPCR) (Vogelstein and Kinzler, 1999) developed using microfluidic chips is becoming a mainstay technology for absolutely quantifying DNA molecules in a variety of applications such as highly accurate gene expression quantification (Warren et al., 2006), detection of genomic diseases (Devonshire et al., 2015; Jarvius et al., 2006; Tsui et al., 2011) and prenatal diagnosis (Fan et al., 2009; Lo et al., 2007; Tsui et al., 2011). Although dPCR has the capability of identifying single DNA molecule, its determination accuracy is still compromised by the misclassification of positive partitions (Jacobs et al., 2014).

Factors that result in the misclassification of positive partitions can be mainly divided into two groups. The first group is called false negatives, which refers to the presence of low-efficient reaction in the positive microchambers causing themselves being regarded as negatives (Whale et al., 2016). The second group is called false positives, including those negative microchambers being considered as positives because water evaporation, cross-contamination or non-specific amplification happen in them (Huggett et al., 2015). Some efforts have been tried on the dPCR data process to reduce the effect of the aforementioned problems on dPCR accuracy (Dreo et al., 2014; Jacobs et al., 2017; Jones et al., 2014; Strain et al., 2013; Trypsteen et al., 2015). Compared to the hard threshold methods at the past, these methods

* Corresponding author at: Research Center for Analytical Instrumentation, Institute of Cyber-Systems and Control, State Key Laboratory of Industrial Control Technology, Zhejiang University, Hangzhou 310027, PR China.
E-mail address: muying@zju.edu.cn (Y. Mu).
[1] These authors contributed equally to this work.

https://doi.org/10.1016/j.bios.2018.12.055
Received 11 December 2018; Received in revised form 21 December 2018; Accepted 25 December 2018
Available online 11 January 2019
0956-5663/

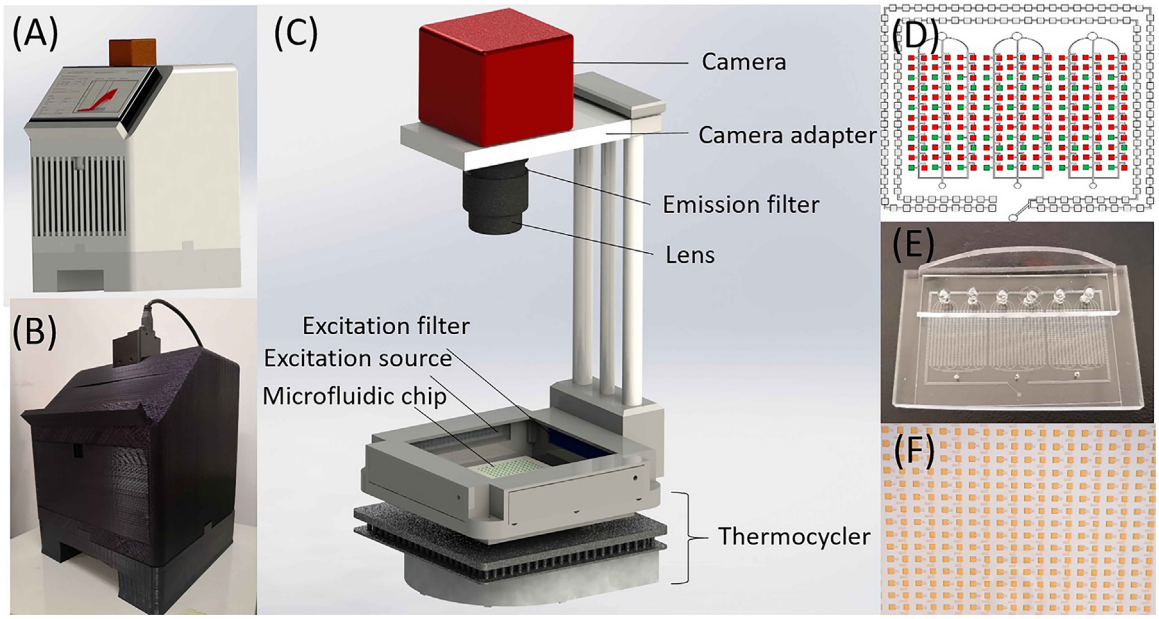

Fig. 1. (A) CAD rendering of real-time dPCR device. (B) The real appearance of the completely assembled device using 3D printing technique. (C) Internal structure of the device. (D) The design detail of the chip. A peripheral water tank was added to prevent evaporation. (E) The real picture of the chip. (F) The image of the chip taken by the microscope after loading the Calcein solution.

perform better on the accuracy. However, these methods only optimize the data from a statistical perspective and have difficulty in differentiating the false signals from the true ones because of the endpoint detection methodology, which limits the further improvement on accuracy.

Real-time fluorescence detection for microfluidic digital array provides the alternative, eventually improving the quantitative accuracy of dPCR. The platforms established using this strategy is termed “real-time dPCR” platforms. The real-time dPCR takes the advantage of real-time quantitative PCR, which can monitor the time-course changes of fluorescence intensity during PCR reaction. Sundberg et al. established a real-time dPCR system based on plastic chip chamber (Sundberg et al., 2010), which reduced the cost of a disposal chip, simplified device complexity and saved the time of thermal cycling. However, the platform only obtained the real time average fluorescence intensity of all microchambers instead of each microchamber. Compared to this platform, Beer et al. reported an on-chip digital microfluidic real-time dPCR device with the ability of realtimely monitoring every droplet within the field of view of the camera (Beer et al., 2007). However, the number of droplets is too low. After that, Hatch et al. released a 1-million droplet array with wide-field fluorescence imaging system (Hatch et al., 2011). Although this highly integrated design yields a 100-fold increase in the number of on-chip digitized reactors, in droplet digital PCR (ddPCR) the droplets tend to move slowly and coalesce to form big ones (Baret, 2012; Chen et al., 2018). So this platform only shows 50 droplets real-time monitoring information. In order to solve this problem, Selck et al. built a custom large-format digital real-time amplification device that can capture each chamber's information (Selck and Ismagilov, 2016). However, the device didn’t use real-time information to improve the accuracy of digital PCR, and the overall volume of the device was large and bulky. In the industry, BioMark™ HD System is a mature platform which can realize both real-time qPCR and real-time dPCR (Baker, 2012). This instrument has been used in a lot of applications (Bhat et al., 2009; Fu et al., 2015; Sanders et al., 2011; Zhu et al., 2016), while it entails the peripheral sampling equipment (Selck and Ismagilov, 2016), which shows high cost. Therefore, the development of highly integrated, inexpensive real-time dPCR device is urgently demanded.

Presented in this work is a highly integrated, affordable design that provides real-time analysis of dPCR reactions. It is able to achieve a high accuracy by differentiating the false signals. All of these were accomplished by integrating rapid self-priming dPCR chip, on-chip thermocycler, real-time fluorescence imaging, and result analysis on a single microfluidic platform, which were automatically controlled by a custom Linux-based application. This device was made of 3D-printed parts and off-the-shelf electronics. The thermocycler we choose was presented by our lab in previous work (Gou et al., 2018), which could provide exact and uniform temperature controlling. The real-time fluorescence imaging of an approximately 12 cm^2 area was achieved using a 10-megapixel camera and 25 mm Lens. All the electronics and tablet were controlled using a single-board computer. Combined with a self-priming dPCR chip previously developed by our laboratory (Zhu et al., 2017), our real-time dPCR device permitted higher quantitative accuracy than the commercial Quantstudio™ 3D dPCR system, when assaying a plasmid DNA containing the human 18S ribosomal RNA gene fragment. Therefore, this real-time dPCR device with high integration and low cost is very helpful to address the misclassification of positive partitions and improve the high accuracy of quantitative analysis. A comparison table in which we compare the performance between our device and others can be found in Table S1.

2. Materials and methods

2.1. System design and instrumentation

The real-time dPCR system mainly consisted of four parts, including: (1) the microfluidic dPCR chip; (2) the thermocycler; (3) the fluorescence image setup; and (4) the Raspberry Pi with the touch screen. A section view of the real-time dPCR system is shown in Fig. 1. Microfluidic dPCR chip acted as a reaction vessel. The thermocycler achieved the precise temperature control in the range of PCR reaction. The fluorescence image setup collected real-time fluorescence images. Moreover, the Raspberry Pi with the touch screen was responsible for system controlling, image processing and data analysis. The overall size of the device was 20 cm × 20 cm × 25 cm. Fig. 1A is the 3D rendering graph of this device's appearance using 3D CAD software (SolidWorks Premium 2017, Dassault Systemes S.A). The device's shell, internal holder and camera adapter were fabricated by 3D-printer (HR0402 3D

printer, China). The actual device is shown in Fig. 1B. A perspective view of the real-time dPCR device is shown in Fig. 1C.

2.2. Microfluidic chips

The dPCR microfluidic chips were designed and fabricated using standard soft lithography technique. Detailed information about the fabrication of the chip was described in the Supporting information. Fig. 1D shows the details of the chip, which contains three reaction panels with 1120 uniform chambers per panel. The sizes of the chip, microchamber array region and microchamber are 4 cm × 3 cm (length × width), 3.5 cm × 1.2 cm (length × width), 150 μm × 150 μm × 230 μm (length × width × height), respectively. The volume of each panel is 5.8 μL. To prevent evaporation of the marginal chambers, a peripheral water tank including two parallel rows of microchambers connected by channels was added, with the size of each microchambers of 150 μm × 150 μm × 230 μm (length × width × height). Fig. 1E shows the real structure of the chip and Fig. 1F describes the details of the channels and reaction chambers.

2.3. Thermocycler

The thermocycler in the real-time dPCR device was presented by our lab in previous work (Gou et al., 2018). A turbo fan (C81H Dayu, PCCOOLER, Shenzhen, China) attached to a steel plate was placed at the bottom of the thermocycler, with a Peltier heater (Ferrotec, Hangzhou, China) being fixed on them. Then, a copper plate coating by heat-conducting silicone grease (HONGDA Latex industry CO., LTD, Liyang, Jiangsu, China) with a temperature sensor (MF52 ZT, Fuwen Sensing CO., LTD, Shenzhen) being embedded into it covered the Peltier heater to assemble as a thermocycler.

2.4. Real-time fluorescence imaging setup

In order to provide uniform and high intensity illumination over full field of view (about 12 cm^2), four long strips of LED with 470 nm center wavelength (60 mm × 8 mm) (Genesis Photonics Inc., China) were placed perpendicular to the surface of the microfluidic chip, horizontally exciting the chip from the side. Then, the excitation light passed through an excitation band pass filter (BPF) (52 mm × 12 mm) (Mega-9 Optoelectronic, China) that has the same size as the LED, with 470 nm center wavelength and 20 nm bandwidth. Being excited by the filtered excitation light, fluorescent reagents in the positive microchambers produced a specific fluorescence that passed through the lens of camera. After that, an emission BPF with a center wavelength of ≈ 550 nm, and a band pass of ≈ 20 nm was used to suppress the residual blue light while let most of the emission light go through the BPF and to be collected by the camera.

The emission BPF was placed between the camera and lens to avoid the interference of light with large incident angles. As the incident angle increases, the center wavelength of filter will move towards the shortwave continuously (Hadley and Dennison, 1947). Thus, losing the ability of removing the residue blue light. In order to strike a balance between good image resolution and inexpensive optical devices, a JHSM1000f camera with a 10-megapixel 1/2.3′ CMOS sensor and a 25 mm f/1.8 manual Lens (Jhtech Inc., China) were used to capture real-time fluorescence images, its CMOS sensor pixel size is 1.67 μm × 1.67 μm, and the resolution is 3664 × 2748. The camera and Lens were mounted on a 3D printing adapter and positioned 20 cm above the thermocycler to obtain a full field of view (approximately 12 cm^2). Image capture settings were taken at f/1.8 aperture, and approximately 6 s exposure in RGB24 image format to achieve efficient collection of weak fluorescence. In addition, there is two white LEDs placed on either side of the thermocycler at a 45° angle for bright-field imaging.

2.5. Digital PCR

To verify the quantitative ability of our device, we carried out dPCR assay to quantify the human 18 S ribosomal RNA gene fragment cloned in a plasmid DNA (Sangon Biotech, China) using our dPCR chip. Each 10 μL reaction mixture consisted of 5 μL of 10 × TaqMan gene expression master mix (Thermofisher Scientific, USA), 0.5 μL of 2% Tween 20, 0.5 μL 18 S ribosomal RNA probe (Thermofisher Scientific, USA), 1 μL template solution, and 3 μL Nuclease-free water. All the reaction mixtures were mixed off-chip before the dPCR reaction.

The complete reaction process was set as follows: first, the chip was degassed in a vacuum pump to evacuate the air dissolved in the PDMS to 0.1 kPa for 20 min. Second, the water tank was filled with water to prevent evaporation of marginal chambers in reaction area. The 10 μL mixture was loaded into the chip under the actuation of negative pressure, then the sealing oil was loaded to separate each microchambers. Third, the dPCR was performed with a program setting as follows: 50 °C heating for 2 min, 95 °C hot start for 10 min, and 60 thermal cycles at 95 °C for 10 s and 60 °C for 60 s. Camera would capture the fluorescence images of the chip during every annealing extension phase of each PCR cycle.

3. Results and discussion

3.1. Real-time fluorescence imaging

The main innovation of our real-time dPCR system is that we collect the real-time fluorescence intensity of each microchamber and use the fluorescence kinetics information to achieve accurate classification of real positive microchambers, which is significant to improve quantitative accuracy of dPCR, especially for low concentrations of the loaded samples. The thermal uniformity of the copper plate of the thermocycler, the intensity distribution of excitation light in microchamber region, the sensibility of CMOS sensor, and the field of view for one-time imaging are important factors affecting the accuracy of experimental results. Based on the previous work published by our laboratory, the temperature of microchamber array in the dPCR chip showed good thermal uniformity with a coefficient of variation (CV) of 0.53% (Gou et al., 2018).

A long strip-shaped high-brightness LED was used as excitation light which streamed from the four sides of the chip parallel to the microchamber area of the chip. Schematic diagram of the optical system is shown in Fig. 2A. This design not only improved the utilization of the excitation light, but also ensured the uniformity of the intensity distribution of excitation light in microchamber region. In order to verify the uniformity of the excitation light intensity in the PDMS chip, optical simulation was performed in the optical design software TracePro (TracePro Expert 7.3.0 Release, Spatial). The result about intensity distribution of the excitation light on the surface of the chip is shown in Fig. 2B. The area of the total microchambers on the chip was about 5 cm^2 and the results of simulation showed that the light intensity on the surface of the chip was roughly a circle with a diameter of 30 mm, covering the almost entire microchambers' area. The average unevenness of the overall light intensity fulfilled the requirement of uniform light in our device. In order to further verify the brightness uniformity of our device, Calcein solution was loaded into the dPCR chip, then taking a fluorescent image of the chip on our device and the Maestro Ex IN VIVO system. As shown in Fig. 2C and Fig. 2D, the two platforms had comparable distribution of fluorescent intensities. Two techniques were used to ensure the consistency of illumination conditions during PCR reaction. First, the "on or off" state of the excitation LEDs were controlled by the Raspberry Pi based on the information acquired by the Bluetooth communication. LEDs were "on" for each primer extension phase in PCR cycles, while LEDs were "off" for the rest of the time. It was a more effective way to weaken the light decay of the LEDs, in comparison with the shutter mode. Second, the LEDs would warm up

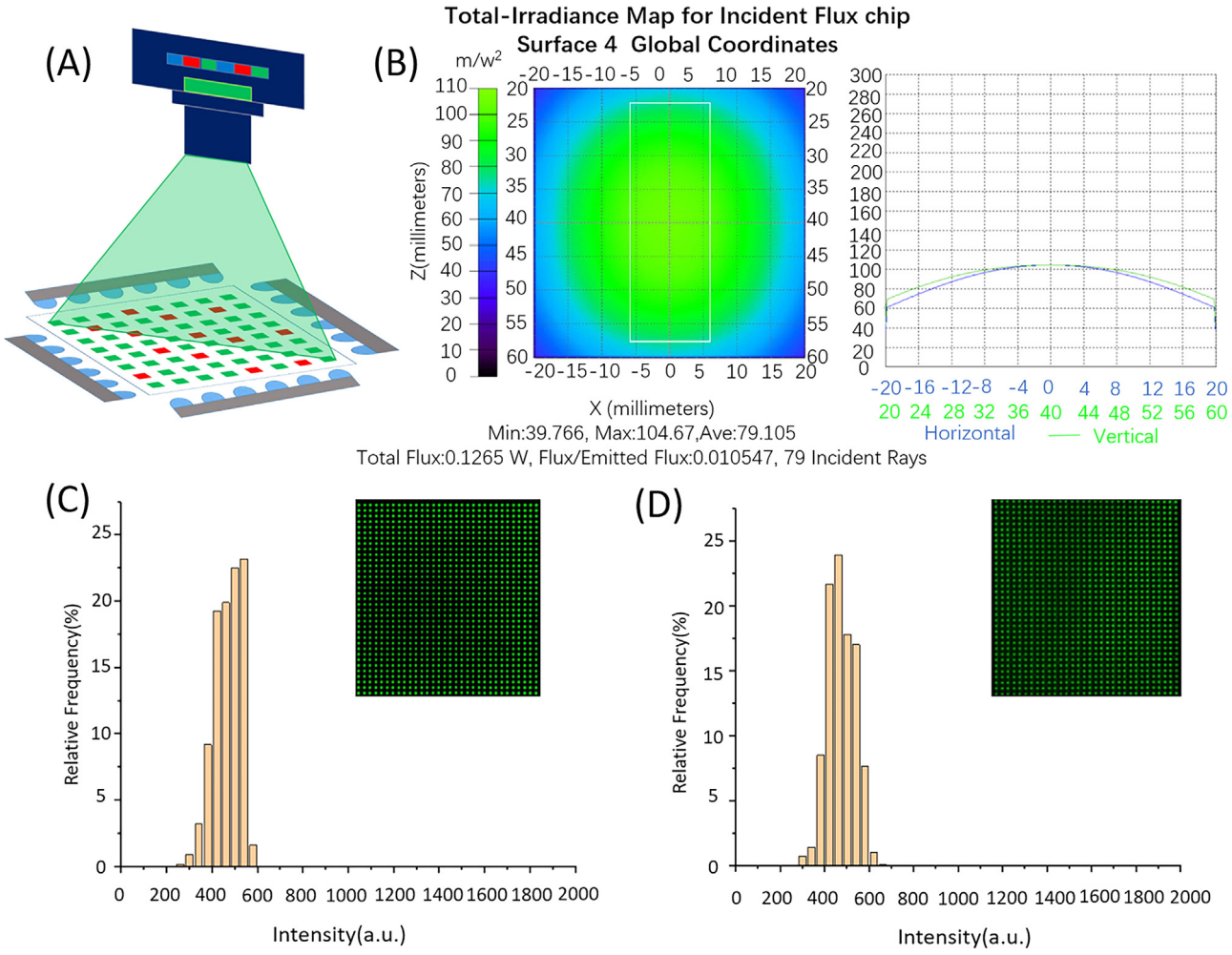

Fig. 2. (A) Schematic diagram of the optical system. The microfluidic chip was side-coupled to two pairs of blue LEDs, ensuring uniform excitation across the chip. An excitation band pass filters (BPF) was placed in front of every LED, which was not shown in the figure. A full-field uniform brightness image (about 12 cm^2) could be obtained at every PCR cycle. (B) Light intensity distribution of the excitation light on the chip area drawn by Tracepro. The white box represented the microchambers' area (about 5 cm^2). (C) And (D) The fluorescence intensity distribution of the chip loaded with Calcein solution using our device and Maestro Ex IN VIVO imaging system. Images in the upper right corner are the fluorescence images of the chip. Histograms represented the fluorescence intensity of every microchamber in fluorescence images, and the results showed that the two images had similar distribution of the fluorescence intensities.

for 10 s after being turned on before the image collecting, which fully utilized the exposure time and kept the LEDs stable. Therefore, this is an economic way to realize the satisfactory excitation condition with sufficient strength and sufficient uniformity.

Cooled CCD sensors have been historically chosen over their CMOS counterparts due to less noise and higher signal gains (Hatch et al., 2011). Scientific complementary metal-oxide semiconductor (sCMOS) camera has high-quality imaging performance of CCD and high-speed readout performance of CMOS (Huang et al., 2013). Many commercial fluorescent microscopes are equipped simultaneously with a cold CCD-level image sensor as a bright-field imaging camera and a sCMOS-level image sensor as a fluorescence-imaging camera. However, their cost is relatively high. CMOS becomes popular gradually because of the improvements of CMOS technology in recent years (El Gamal and Eltoukhy, 2005). JHSM1000f camera with a 10-megapixel 1/2.3′ CMOS sensor was chosen in this experiment, which can capture 3360 microchambers in a 12 cm^2 viewing area in a single snap. With these imaging parameters, about 170 pixels per microchamber resolution could be achieved. The change over time of the overall fluorescence intensity of the real-time fluorescence image could be clearly discerned by the naked eyes, as shown in Fig. 3. A 25 mm focal length C-type interface lens was used to balance the request of image fidelity and imaging distance for our chip. The total price of the camera, the lens, raspberry pi and touch screen in our system is only equivalent to the price of a regular smartphone.

3.2. Data collection and analysis software

A Linux-based application for Raspberry Pi was developed in C++ based on Qt Creator and had three main functions: real-time fluorescence image acquisition, fluorescence image processing (creating a mask), and image data analysis. Since Qt Creator is a cross-platform Qt integrated development environment, this application is also suitable for Windows systems. The Raspberry Pi's onboard Bluetooth (Bluetooth 4.2, BLE) communicated with the Bluetooth on the thermocycler, and the application used the information obtained from Bluetooth communication to perform precise and fast three-temperature loop control of the thermocycler. Meanwhile, the Raspberry Pi controlled the cooperation of camera and LEDs to complete the fluorescence image acquisition during the annealing extension phase of each PCR cycle. After the end of the PCR cycle, all of images were saved in a specified address. In order to improve the efficiency, all images were scaled before the image processing, so that the fluorescence intensity of each microchamber in the paper was obtained from resized images. The image processing mainly contained the following steps: seed image acquisition, image preprocessing, acquisition of regions of interest (ROI),

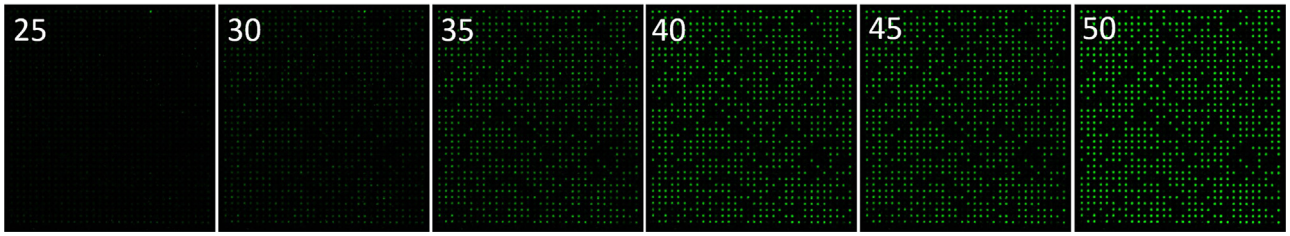

Fig. 3. Real-time dPCR results using the self-priming microfluidic dPCR chip. The fluorescence images were captured every five cycles from cycle 25–50, with the sample concentration of 2000 copies/μL. Real-time dPCR results of other sample concentrations are shown in Fig. S4.

microchamber coarse positioning, microchamber precise positioning and mask creation (See Supplementary information for more details).

Using the microchamber position information in the mask and the image traversal function of application, we got the fluorescence intensity of each microchamber per cycle (the G channel value of each pixel of the selected image represented the fluorescence intensity), then plotted the real-time fluorescence curve of each microchamber. Afterwards, we chose polynomial fitting method to achieve curve fitting. Different types of curves corresponded to different types of microchambers. According to the characteristics of the fitted curves, they were classified easily, quickly and accurately into negative microchamber (non-target reactions), positive microchamber (one or more than one target-containing reactions), evaporating microchamber (water evaporating reactions), false positive microchamber (nonspecific amplifications or other unknown reason), respectively. The characteristics of these four types of microreactors are as follows: no significant change in fluorescence signals, S-type amplification, having a rapid increase of fluorescence signals between adjacent cycles, and S-type amplification with a delayed exponential growth. Then we could achieve accurate quantification of the sample solution, Fig. 4 shows the process of curve classification. In order to achieve better human-computer interaction, the application system developed a graphical user interface. The interface included three pages: real-time experiment page, mask creation page, and image data analyze page. Each page was provided with parameter input and parameter display area, function button area, image display area and other areas. The detailed information about this application interface is showed in Fig. S2. The integration of Raspberry Pi's single-board computer and capacitive screen in the system reduced the volume of the device and improved system integration and portability to some extent. The Raspberry Pi's single-board computer was able to process the real-time experiments data (Mendoza-Gallegos et al., 2018; Stephenson et al., 2018; Xu et al., 2018). Moreover, it enabled the device more affordable and user-friendly than other currently available real-time dPCR systems.

3.3. Real-time digital PCR validation

In order to validate the stability and accuracy of our real-time dPCR device, we used a stock plasmid DNA of 10^7 copies/μL containing the 18 S ribosomal RNA gene fragment with the different gradients concentration to perform real-time dPCR: 1×10 copies/μL, 1×10^2 copies/μL, 1×10^3 copies/μL, 2×10^3 copies/μL, respectively. The concentration of synthetic plasmid DNA sample was measured using Qubit 3.0 Fluorometer (Life technologies, USA). Then this original sample was diluted to 10^7 copies/μL. The real-time fluorescence images of PCR amplification of concentration 2×10^3 copies/μL between cycles 25–50 in 5 cycle increments are shown in Fig. 3 (See Fig. S4 for more information). The amplification plots (left) and the panel hot maps (right) of NTC and four concentration gradients are shown in Fig. 5. The baseline-corrected tracing of amplification from each microchamber in the microfluidic device (left image of each group of diagrams) reflects the change of fluorescence intensity. The characteristics of fluorescence change curves were vital to accurately classify microchambers. The software-generated panel hot map (right image of each group of diagrams) visually shows the actual reaction circumstance of the each microchamber. As reported previously (Xu et al., 2018), the sampling loading in our self-priming dPCR chip conforms to Possion Distribution. Therefore, we introduced Poisson distribution to calculate the DNA templates. According to the formula:

$$P(n, \lambda) = \lambda^n e^{-\lambda}/n!, \quad \lambda = 0, \quad 1, \quad 2..., \tag{1}$$

Where n is the number of DNA molecules per microchamber and λ refers to the ratio of the total number of target DNA molecules to the number of reaction chambers. If a microchamber presents the enhancement of fluorescent signal, then it shows that there is at least one target molecule within this chamber. Therefore, the ratio between fluorescent microchambers and total number of microchambers f_0 is equal to the possibility of a chamber occupying at least one target DNA template. So,

$$f_0 = P(n > 0, \quad \lambda) = 1 - P(n = 0, \quad \lambda) = 1 - e^{-\lambda} \tag{2}$$

And then,

$$-\ln(1-f_0) = \lambda \tag{3}$$

In our dPCR system, 1 μL serially diluted DNA template was added into 10 μL reaction mixture. 5.8 μL of 10 μL reaction mixture was remained in the microchambers, therefore,

$$\lambda = \left(C_0 \times X_{dil} \times 1 \times \frac{5.8}{10}\right)/N \tag{4}$$

Where C_0 refers to the concentration of stock DNA template and X_{dil} is dilution factor. For example, the X_{dil} for 1×10^3 copies/μL is 10^{-4}. And N is 1120.

And then,

$$-\lg(-\ln(1-f_0)) = -\lg 0.58 X_{dil} - \lg\left(\frac{C_0}{N}\right) \tag{5}$$

Therefore, there is a linear relationship between –lg (–ln (1-f_0)) and –lg 0.58 $\times_{dil}$, and C_0 can be calculated using the intercept. As shown in Fig. 5F, the liner fitting curve equation was $Y = 1.004 \times -3.981$ (R^2 = 0.9998), from which we could calculate that the original concentration of target was $1.07 \times 10^7 \pm 1242$ copies/μL (Table S2). Also, the total DNA concentrations we obtained using our real-time dPCR device closely matched the predicted outcomes. In addition, we also applied end-point dPCR on our device, the detailed image processing and the results are shown in the Fig. S3. For further comparison, the parallel test using Quantstudio™ 3D dPCR system were carried out to assay the same plasmid DNA targets with three orders of magnitude from $1{:}10^4$ to $1{:}10^6$. As shown in Fig. 6 (See Supplementary information for details), the results of the real-time dPCR on our device was better matched with predicted outcomes than the results of the end-point dPCR on our device and the commercial digital PCR. Moreover, the results of our real-time dPCR device clearly identified the negative microchambers, positive microchambers, evaporating microchambers, false positive microchambers, respectively, providing a more convincing value of concentration of the sample. Therefore, our real-time dPCR device is helpful to improve the quantitative accuracy of dPCR.

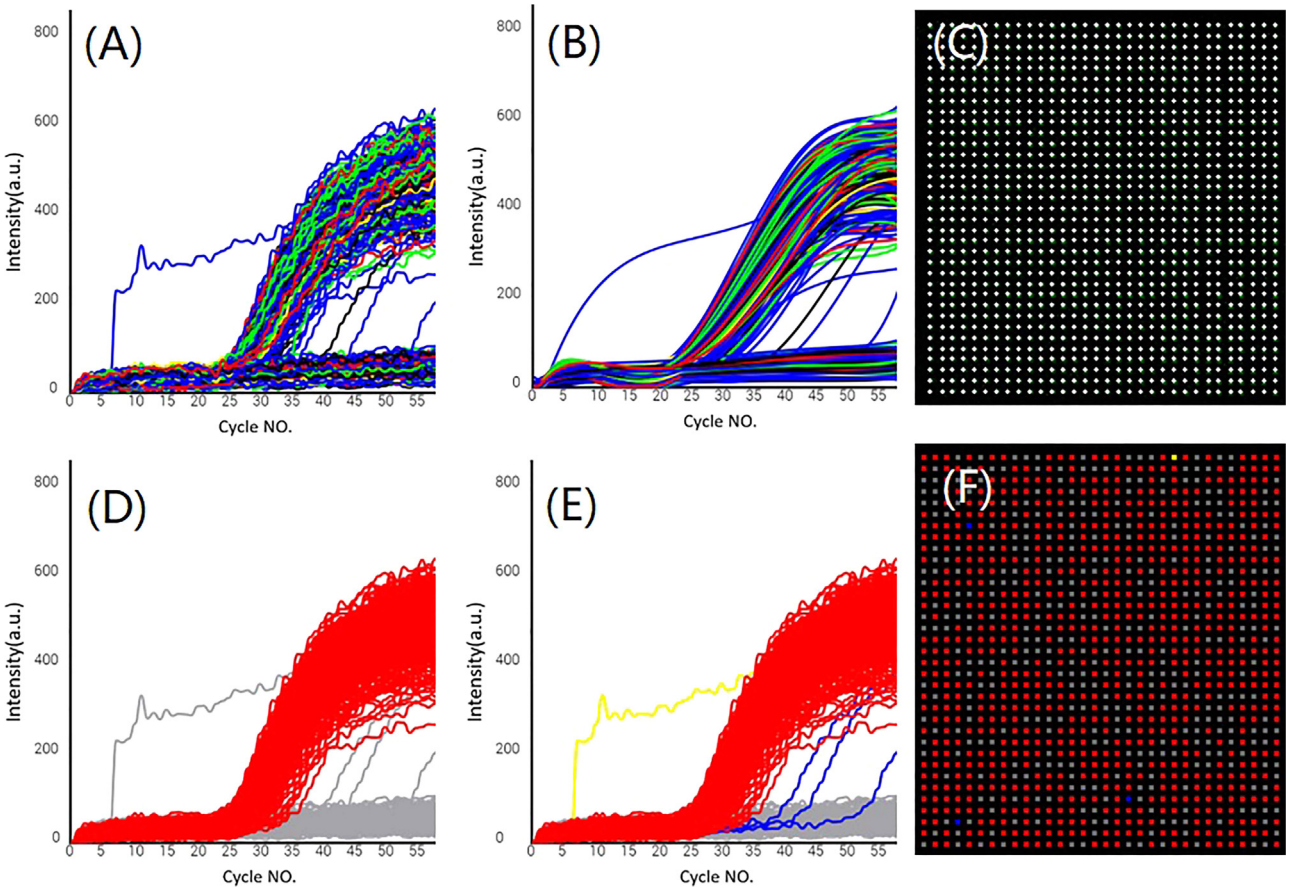

Fig. 4. Precise curve classification based on curves' characteristics. (A) The real-time fluorescence intensity curves of every microchamber in the (C). (B) Fitted curves according to the real-time fluorescence intensity curves. The fitting method is a polynomial fitting and the maximum number of polynomial terms is 5. (C) Microchambers location of the ROI in the complete seed image. (D) The curves are divided into two kinds of types, in which red curves stand for positive microchambers and grey ones refer to negative microchambers. (E) The curves are divided into four kinds of types, in which blue ones are false positive microchamber and yellow ones are evaporating microchambers. (F) The software generates the panel hot map according to the information from the (E), and the color of the square is consistent with the curve.

4. Conclusion

In this paper, we have presented a highly integrated and low-cost real-time dPCR device that significantly increases the accuracy of dPCR. Three samples can be detected at a time by using dPCR chip we mentioned above. In addition, the throughput of our device can be enlarged using other microfluidic dPCR chips with more microchambers, or the droplet digital PCR (ddPCR) chip with thermosetting oil developed by our lab (Wu et al., 2018). Real-time dPCR for microfluidic arrays was successfully achieved with uniform amplification in each microchamber. Besides, the illumination setup of the device was designed to be composed of easily obtainable illumination and optical components, which provides a high and uniform illumination intensity over full field of view (about 12 cm^2). Moreover, the fluorescence image processing and data analysis were easily achieved. All the function units were automatically controlled by the supplementary application we developed. Thus, our system is more compact and more economical than other existing real-time dPCR systems. An itemized list, including cost of each component can be found in Table S4.

Compared with the end-point detection on our device or the commercialized Quantstudio™ 3D dPCR system, the real-time detection on our device shows higher accuracy on quantifying the human 18S ribosomal RNA gene sequence. The real-time dPCR presented here not only provides a new way to solve the problem of misclassification of positive partitions, but also gives the information about the kinetics of amplification on digital microfluidic devices, both of which are useful for improving the quantitative accuracy of dPCR. In the future, our real-time dPCR device will be upgraded by integrating the sample pretreatment unit (Chen and Li, 2017; Chen and Zhang, 2017; Sun et al., 2018) to achieve the "sample-in and answer-out" detection format (Fu et al., 2017; Hu et al., 2017; Song et al., 2018) and adding extra optical accessories to fulfill multi-channel (Anazawa and Yamazaki, 2017) extension. Our lab has developed an integrated microfluidic device with nucleic acid extraction functional module (Tian et al., 2015), we could add several micro-pumps and micro-valves to realize automatic injection. Also, we will equip multi-band light source, suitable filter set, and automated structure, enabling our device to capture multicolor fluorescent image after every PCR cycle.

In conclusion, our developed highly-integrated and low-cost real-time dPCR device is anticipated to be useful for applications such as rare mutation detection, GMO quantitation, and aneuploidy detection, in which false positives are intolerable and accuracy is paramount.

Acknowledgements

The authors thank the funds from the National Natural Science Foundation of China (81741145), the National Key Foundation for Exploring Scientific Instruments (2018YFF01012100) and the Open Research Project of the State Key Laboratory of Industrial Control Technology, Zhejiang University, China (No. ICT1800418).

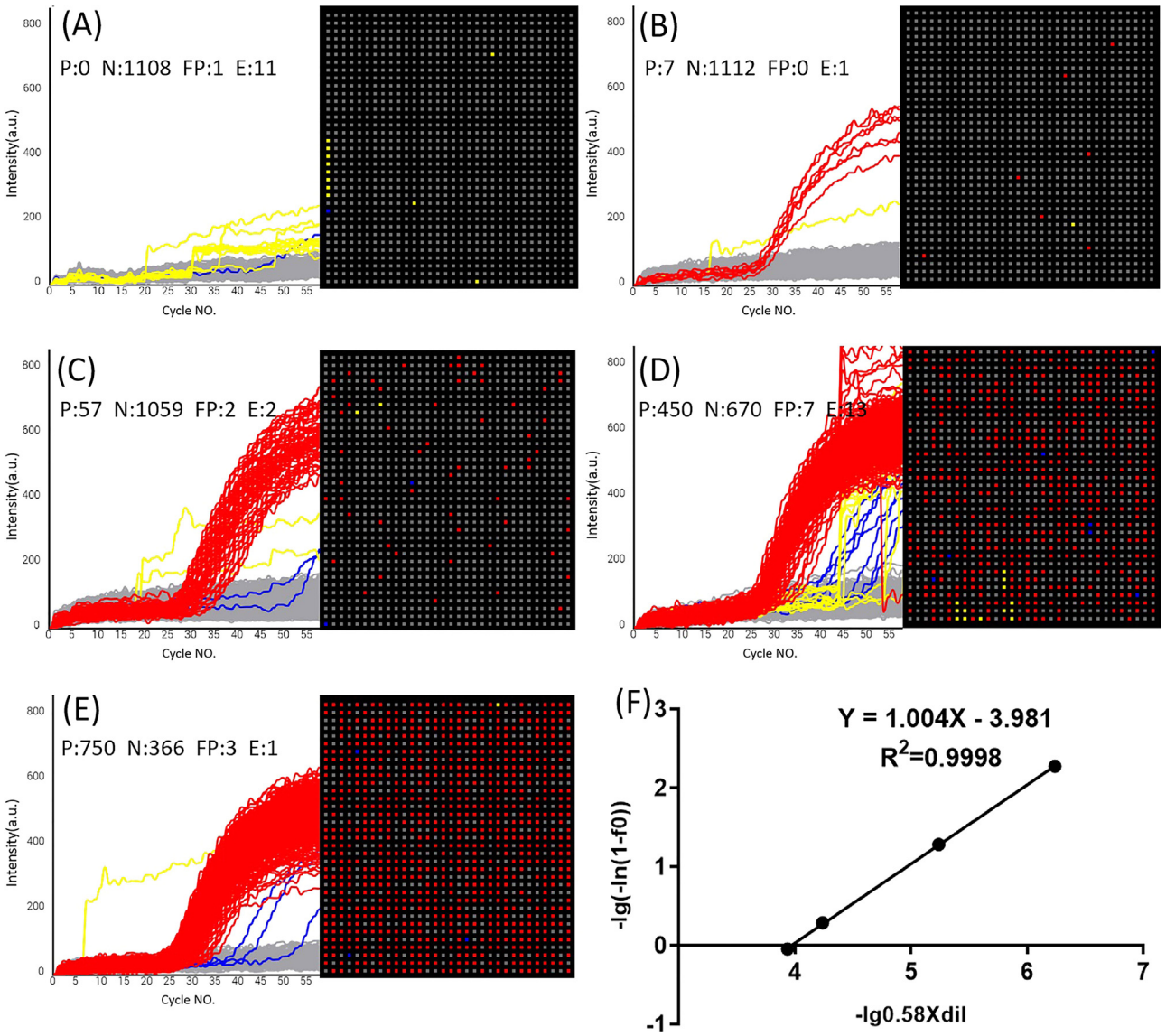

Fig. 5. (A-E) The amplification plots (left image of each group of diagrams) and the panel hot map (right image of each group of diagrams) show the results of curve classification and DNA quantification. Each curve reflects the change in fluorescence intensity of each microchamber. Each square in hot map visually shows the actual reaction circumstance of the each microchamber. (F) A regression curve of human 18 S ribosomal RNA gene fragment was acquired by plotting –lg (− ln (1 − f_0)) against the dilution factor –lg0.58 $\times_{dil}$.

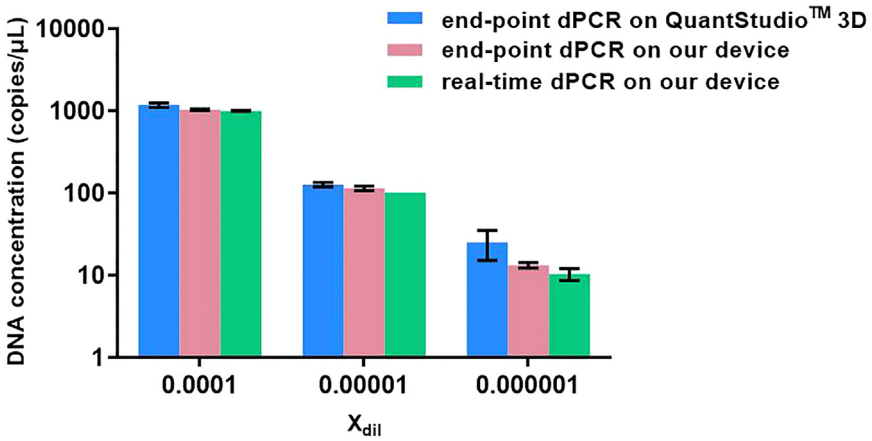

Fig. 6. Comparison of QuantStudio™ 3D dPCR system, end-point dPCR on our device and real-time dPCR on our device quantification results of copy number for human 18S ribosomal RNA gene fragment detection with three concentrations of 10 copies/μL,100 copies/μL, 1000 copies/μL, respectively.

Credit author statement

Shufang Zhou and Tong Gou designed the optical system, thermocycler and assembled them into a real-time dPCR device. Shufang Zhou developed the software and Weibo Fang provided assistance in this work. Shufang Zhou and Jiumei Hu conducted the dPCR validation experiments. Ying Mu and Wenshuai Wu provided guidance. Shufang Zhou, Xiong Ding, Jiumei Hu, Wenshuai Wu and Tong Gou wrote and revised the paper. Shufang Zhou, Jiumei Hu and Zhenming Hu fabricated the microfluidic chips. All co-authors reviewed and approved the manuscript.

Conflicts of interest

There are no conflicts to declare.

Declaration of interests

None.

Appendix A. Supplementary material

Supplementary data associated with this article can be found in the online version at doi:10.1016/j.bios.2018.12.055

References

Anazawa, T., Yamazaki, M., 2017. An ultra-small, multi-point, and multi-color photodetection system with high sensitivity and high dynamic range. Lab Chip 17 (24), 4231–4242.

Baker, M., 2012. Digital PCR hits its stride. Nat. Methods 9 (6), 541–544.

Baret, J.C., 2012. Surfactants in droplet-based microfluidics. Lab Chip 12 (3), 422–433.

Beer, N.R., Hindson, B.J., Wheeler, E.K., Hall, S.B., Rose, K.A., Kennedy, I.M., Colston, B.W., 2007. On-chip, real-time, single-copy polymerase chain reaction in picoliter droplets. Anal. Chem. 79 (22), 8471–8475.

Bhat, S., Herrmann, J., Armishaw, P., Corbisier, P., Emslie, K.R., 2009. Single molecule detection in nanofluidic digital array enables accurate measurement of DNA copy number. Anal. Bioanal. Chem. 394 (2), 457–467.

Chen, J., Luo, Z., Li, L., He, J., Li, L., Zhu, J., Wu, P., He, L., 2018. Capillary-based integrated digital PCR in picoliter droplets. Lab Chip 18 (3), 412–421.

Chen, X.Y., Li, T.C., 2017. A novel passive micromixer designed by applying an optimization algorithm to the zigzag microchannel. Chem. Eng. J. 313, 1406–1414.

Chen, X.Y., Zhang, L., 2017. A review on micromixers actuated with magnetic nanomaterials. Microchim. Acta 184 (10), 3639–3649.

Devonshire, A.S., Honeyborne, I., Gutteridge, A., Whale, A.S., Nixon, G., Wilson, P., Jones, G., McHugh, T.D., Foy, C.A., Huggett, J.F., 2015. Highly reproducible absolute quantification of mycobacterium tuberculosis complex by digital PCR. Anal. Chem. 87 (7), 3706–3713.

Dreo, T., Pirc, M., Ramsak, Z., Pavsic, J., Milavec, M., Zel, J., Gruden, K., 2014. Optimising droplet digital PCR analysis approaches for detection and quantification of bacteria: a case study of fire blight and potato brown rot. Anal. Bioanal. Chem. 406 (26), 6513–6528.

El Gamal, A., Eltoukhy, H., 2005. CMOS image sensors. IEEE Circuits Device 21 (3), 6–20.

Fan, H.C., Blumenfeld, Y.J., El-Sayed, Y.Y., Chueh, J., Quake, S.R., 2009. Microfluidic digital PCR enables rapid prenatal diagnosis of fetal aneuploidy. Am. J. Obstet. Gynecol. 200 (5).

Fu, W., Zhu, P., Wang, C., Huang, K., Du, Z., Tian, W., Wang, Q., Wang, H., Xu, W., Zhu, S., 2015. A highly sensitive and specific method for the screening detection of genetically modified organisms based on digital PCR without pretreatment. Sci. Rep. 5, 12715.

Fu, Y., Zhou, X.M., Xing, D., 2017. Lab-on-capillary: a rapid, simple and quantitative genetic analysis platform integrating nucleic acid extraction, amplification and detection. Lab Chip 17 (24), 4334–4341.

Gou, T., Hu, J., Wu, W., Ding, X., Zhou, S., Fang, W., Mu, Y., 2018. Smartphone-based mobile digital PCR device for DNA quantitative analysis with high accuracy. Biosens. Bioelectron. 120, 144–152.

Hadley, L.N., Dennison, D.M., 1947. Reflection and transmission interference filters. J. Opt. Soc. Am. 37 (6), 451–465.

Hatch, A.C., Fisher, J.S., Tovar, A.R., Hsieh, A.T., Lin, R., Pentoney, S.L., Yang, D.L., Lee, A.P., 2011. 1-Million droplet array with wide-field fluorescence imaging for digital PCR. Lab Chip 11 (22), 3838–3845.

Hu, B.F., Li, J.J., Mou, L., Liu, Y., Deng, J.Q., Qian, W., Sun, J.S., Cha, R.T., Jiang, X.Y., 2017. An automated and portable microfluidic chemiluminescence immunoassay for quantitative detection of biomarkers. Lab Chip 17 (13), 2225–2234.

Huang, F., Hartwich, T.M., Rivera-Molina, F.E., Lin, Y., Duim, W.C., Long, J.J., Uchil, P.D., Myers, J.R., Baird, M.A., Mothes, W., Davidson, M.W., Toomre, D., Bewersdorf, J., 2013. Video-rate nanoscopy using sCMOS camera-specific single-molecule localization algorithms. Nat. Methods 10 (7), 653–658.

Huggett, J.F., Cowen, S., Foy, C.A., 2015. Considerations for digital PCR as an accurate molecular diagnostic tool. Clin. Chem. 61 (1), 79–88.

Jacobs, B.K.M., Goetghebeur, E., Clement, L., 2014. Impact of variance components on reliability of absolute quantification using digital PCR. BMC Bioinforma. 15.

Jacobs, B.K.M., Goetghebeur, E., Vandesompele, J., De Ganck, A., Nijs, N., Beckers, A., Papazova, N., Roosens, N.H., Clement, L., 2017. Model-based classification for digital PCR: your umbrella for rain. Anal. Chem. 89 (8), 4461–4467.

Jarvius, J., Melin, J., Goransson, J., Stenberg, J., Fredriksson, S., Gonzalez-Rey, C., Bertilsson, S., Nilsson, M., 2006. Digital quantification using amplified single-molecule detection. Nat. Methods 3 (9), 725–727.

Jones, M., Williams, J., Gartner, K., Phillips, R., Hurst, J., Frater, J., 2014. Low copy target detection by Droplet Digital PCR through application of a novel open access bioinformatic pipeline, 'definetherain'. J. Virol. Methods 202, 46–53.

Lo, Y.M.D., Lun, F.M.F., Chan, K.C.A., Tsui, N.B.Y., Chong, K.C., Lau, T.K., Leung, T.Y., Zee, B.C.Y., Cantor, C.R., Chiu, R.W.K., 2007. Digital PCR for the molecular detection of fetal chromosomal aneuploidy. Proc. Natl. Acad. Sci. USA 104 (32), 13116–13121.

Mendoza-Gallegos, R.A., Rios, A., Garcia-Cordero, J.L., 2018. An affordable and portable thermocycler for real-time PCR made of 3D-printed parts and off-the-shelf electronics. Anal. Chem. 90 (9), 5563–5568.

Sanders, R., Huggett, J.F., Bushell, C.A., Cowen, S., Scott, D.J., Foy, C.A., 2011. Evaluation of digital PCR for absolute DNA quantification. Anal. Chem. 83 (17), 6474–6484.

Selck, D.A., Ismagilov, R.F., 2016. Instrument for real-time digital nucleic acid amplification on custom microfluidic devices. PLoS One 11 (10), e0163060.

Song, J.Z., Pandian, V., Mauk, M.G., Bau, H.H., Cherry, S., Tisi, L.C., Liu, C.C., 2018. Smartphone-based mobile detection platform for molecular diagnostics and spatiotemporal disease mapping. Anal. Chem. 90 (7), 4823–4831.

Stephenson, W., Donlin, L.T., Butler, A., Rozo, C., Bracken, B., Rashidfarrokhi, A., Goodman, S.M., Ivashkiv, L.B., Bykerk, V.P., Orange, D.E., Darnell, R.B., Swerdlow, H.P., Satija, R., 2018. Single-cell RNA-seq of rheumatoid arthritis synovial tissue using low-cost microfluidic instrumentation. Nat. Commun. 9 (1), 791.

Strain, M.C., Lada, S.M., Luong, T., Rought, S.E., Gianella, S., Terry, V.H., Spina, C.A., Woelk, C.H., Richman, D.D., 2013. Highly precise measurement of HIV DNA by droplet digital PCR. PLoS One 8 (4), e55943.

Sun, Y., Yuan, J.C., Pang, J.L., Li, X.N., Wang, S.M., Zhou, Y.L., Xu, F., Li, P.C.H., Jiang, S.S., Chen, H., 2018. Millifluidic chip with a modular design used as a sample pretreatment cartridge for flour and flour food products. Talanta 179, 719–725.

Sundberg, S.O., Wittwer, C.T., Gao, C., Gale, B.K., 2010. Spinning disk platform for microfluidic digital polymerase chain reaction. Anal. Chem. 82 (4), 1546–1550.

Tian, Q.C., Mu, Y., Xu, Y.N., Song, Q., Yu, B.W., Ma, C.C., Jin, W., Jin, Q.H., 2015. An integrated microfluidic system for bovine DNA purification and digital PCR detection. Anal. Biochem. 491, 55–57.

Trypsteen, W., Vynck, M., De Neve, J., Bonczkowski, P., Kiselinova, M., Malatinkova, E., Vervisch, K., Thas, O., Vandekerckhove, L., De Spiegelaere, W., 2015. ddpcRquant: threshold determination for single channel droplet digital PCR experiments. Anal. Bioanal. Chem. 407 (19), 5827–5834.

Tsui, N.B.Y., Kadir, R.A., Chan, K.C.A., Chi, C., Mellars, G., Tuddenham, E.G., Leung, T.Y., Lau, T.K., Chiu, R.W.K., Lo, Y.M.D., 2011. Noninvasive prenatal diagnosis of hemophilia by microfluidics digital PCR analysis of maternal plasma DNA. Blood 117 (13), 3684–3691.

Vogelstein, B., Kinzler, K.W., 1999. Digital PCR. Proc. Natl. Acad. Sci. USA 96 (16), 9236–9241.

Warren, L., Bryder, D., Weissman, I.L., Quake, S.R., 2006. Transcription factor profiling in individual hematopoietic progenitors by digital RT-PCR. Proc. Natl. Acad. Sci. USA 103 (47), 17807–17812.

Whale, A.S., Huggett, J.F., Tzonev, S., 2016. Fundamentals of multiplexing with digital PCR. Biomol. Detect Quantif. 10, 15–23.

Wu, W., Zhou, S., Hu, J., Wang, G., Ding, X., Gou, T., Sun, J., Zhang, T., Mu, Y., 2018. A thermosetting oil for droplet-based real-time monitoring of digital PCR and cell culture. Adv. Funct. Mater. 28 (39).

Xu, Y.N., Hu, J.M., Zhu, Q.Y., Song, Q., Mu, Y., 2018. Co-detection of ALDH1A1, ABCG2, ALCAM and CD133 in three A549 subpopulations at the single cell level by one-step digital RT-PCR. Integr. Biol. 10 (6), 364–369.

Zhu, P., Wang, C., Huang, K., Luo, Y., Xu, W., 2016. A novel pretreatment-free duplex chamber digital PCR detection system for the absolute quantitation of GMO samples. Int. J. Mol. Sci. 17 (3), 402.

Zhu, Q., Xu, Y., Qiu, L., Ma, C., Yu, B., Song, Q., Jin, W., Jin, Q., Liu, J., Mu, Y., 2017. A scalable self-priming fractal branching microchannel net chip for digital PCR. Lab Chip 17 (9), 1655–1665.